A novel feature ranking algorithm for biometric recognition with PPG signals

Article *in* Computers in Biology and Medicine · March 2014

DOI: 10.1016/j.compbiomed.2014.03.005 · Source: PubMed

3 authors, including:

Ahmet Reşit Kavsaoğlu
Karabuk University
7 PUBLICATIONS **20** CITATIONS

SEE PROFILE

Kemal Polat
Abant İzzet Baysal Üniversitesi
112 PUBLICATIONS **2,248** CITATIONS

SEE PROFILE

Computers in Biology and Medicine 49 (2014) 1–14

Contents lists available at ScienceDirect

Computers in Biology and Medicine

journal homepage: www.elsevier.com/locate/cbm

A novel feature ranking algorithm for biometric recognition with PPG signals

A. Reşit Kavsaoğlu [a], Kemal Polat [b,*], M. Recep Bozkurt [a]

[a] Department of Electrical and Electronics Engineering, Faculty of Engineering, Sakarya University, M6 Building, 54187 Sakarya, Turkey
[b] Department of Electrical and Electronics Engineering, Faculty of Engineering and Architecture, Abant Izzet Baysal University, 14280 Bolu, Turkey

ARTICLE INFO

Article history:
Received 28 November 2013
Accepted 10 March 2014

Keywords:
Biometrics
Photoplethysmography (PPG)
Identification
Classification
Derivatives
Feature Extraction

ABSTRACT

This study is intended for describing the application of the Photoplethysmography (PPG) signal and the time domain features acquired from its first and second derivatives for biometric identification. For this purpose, a sum of 40 features has been extracted and a feature-ranking algorithm is proposed. This proposed algorithm calculates the contribution of each feature to biometric recognition and collocates the features, the contribution of which is from great to small. While identifying the contribution of the features, the Euclidean distance and absolute distance formulas are used. The efficiency of the proposed algorithms is demonstrated by the results of the k-NN (k-nearest neighbor) classifier applications of the features. During application, each 15-period-PPG signal belonging to two different durations from each of the thirty healthy subjects were used with a PPG data acquisition card. The first PPG signals recorded from the subjects were evaluated as the 1st configuration; the PPG signals recorded later at a different time as the 2nd configuration and the combination of both were evaluated as the 3rd configuration. When the results were evaluated for the k-NN classifier model created along with the proposed algorithm, an identification of 90.44% for the 1st configuration, 94.44% for the 2nd configuration, and 87.22% for the 3rd configuration has successfully been attained. The obtained results showed that both the proposed algorithm and the biometric identification model based on this developed PPG signal are very promising for contactless recognizing the people with the proposed method.

1. Introduction

The fact that today security comes into prominence more and more each day brings the need for one to keep in his/her mind much further and complicated codes and carry extra cards with him/her and that this situation is getting far from practicality and reliability boosts the need for biometric identification. Today most of the systems like financial transactions, computer networks and access into secure places still recognize the authorized people via the identification card and password. Such systems are not secure enough because of the fact that information can easily be stolen and forgotten. Biometric systems are able to provide more reliability and privacy since they work with the principle of identifying the physical and behavioral characteristics of a person which are possessed only by that person himself/herself and which distinguish him/her from others [1].

Certain distinctive features of our body or behavioral attributes, such as finger print, face [2,3], voice [4], retina/iris [5], lip movements [6], walking style [7], electroencephalography (EEG) [8] and electrocardiography (ECG) [9,10] are viewed as means of human identification. These applications based on biometric approaches will provide us with a promising and irrefutable future of human recognition. However, a finger print can be characterized with latex, face recognition can be faked with a photograph, voice can be imitated [11], and the EEG and ECG-based methods are impractical as various electrodes are required in order to acquire bio-signals.

PPG is a non-invasive electro-optical method which gives information about the volume of blood flowing through a testing zone of the body, close to the skin. In order to acquire PPG signal, a source of light, the wavelength of which is λ, is placed on one side of a jut of the body (e.g. a finger) and on the other side, a photo-detector is placed right across the source to see the transmitted light. A typical PPG signal consists of a large DC component passing through the skin, muscle and bone without passing through the blood vessels, a small AC component passing directly through the blood vessels by detaching itself from the skin, muscle and bone and also a light passing through the arterial blood vessels. Shortly after the systole, the amount of blood in the arteries increase, thus the intensity of light received decreases. During the diastole, the amount of blood in the arteries decrease and an increase in the light transmittance is observed. On a basic

* Corresponding author. Tel: +90 530 561 9226; fax: +90 374 253 4558.
E-mail address: kemal_polat2003@yahoo.com (K. Polat).

http://dx.doi.org/10.1016/j.compbiomed.2014.03.005
0010-4825/

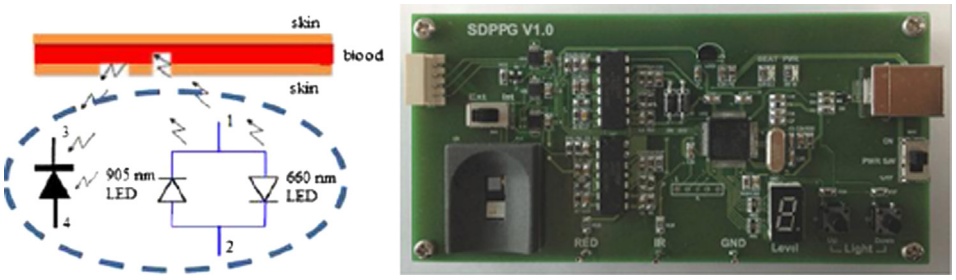

Fig. 1. The schematic diagram of the DCM03 reflective sensor and the PPG signal-acquisition card [13].

measurement zone, 99% of the signal comes from the skin, muscle and bone while 0.9% from the veins and 0.1% from the arteries [12]. In Fig. 1, the schematic diagram of the DCM03 reflective sensor used for acquiring the PPG signal and a PPG signal-acquisition card are seen [13].

The recommended method in this study comprises the new feature extractions with PPG signals aiming at biometric recognition, data acquisition, pre-processing, PPG signaling and the feature extraction of PPG signal using its first and second derivatives, the recommendation of a feature ranking algorithm by analyzing the contribution of the extracted features to biometric recognition and the *k-nearest neighbor* classification processes. The process of data acquisition was provided by 30 volunteers through a PPG data acquisition card. Various artifacts like analog circuit noises to be found in the signal acquired by pre-processing, medium illuminance change, respiration and base deviation arising from movement are eliminated. 40 features of PPG signal in the time domain, such as systolic peak, diastolic peak, augmentation index, peak-to-peak interval and pulse width were found using the PPG signal and its derivates. For each of these features, feature ranking process was performed by separately calculating their contribution to biometric recognition. The first 5, 10, 15, 20, 25, 30, 35 and 40 of the ranked features were selected, and the *k-nearest neighbor* classification method was used for each of them separately.

2. Related works

In their studies, Gu et al. offer a new approach of human verification using the PPG signals acquired easily from the fingertips. They performed their experimental studies on a group of 17 healthy subjects. They obtained four feature parameters from digitized PPG signals. A feature vector template was formulated using the recorded signals, and later on, the discriminant function was applied in order to verify the data. This promising method of human identification finally achieved a 90% success [1]. In another study, two important inferences like the derivatives of PPG signals, and the consistency of subjects within themselves and the distinguishability among different subject are examined. Experimental results suggest that using statistical instruments, the derivatives can certainly indicate the features of one's PPG signal and can be used as biometrics for recognition [14].

In another study, on the other hand, the feasibility of the application of PPG signal as a single biometrical feature along with the signal-processing methods for the matter involved are being researched. The PPG signals were acquired from the fingertips of 29 healthy subjects. The experimental results suggest that when PPG signals come under a controlled environment with infallible sensors, biometrics for identification can also be used [15].

Wei et al., in their studies, addressed that PPG signals could reflect numerous physiological parameters, such as heart functions, blood vascular elasticity and blood viscosity. This is a new non-invasive method with the advantages like smoothness and accuracy. It is important to find out efficient pre-processing and feature extraction algorithms in order to deal with the original PPG signal that could be affected by many other factors. Most of the practical methods include median and FIR (finite infinite response) filtration. In this study, a new algorithm is recommended in order to eliminate the wavelet transform-based baseline deviation. The inference of feature spots is another important issue. A sophisticated differential algorithm is used to solve this problem. All these practical algorithms have created an effective platform for determining the physiological parameters.[16]

Gu et al., in another study of theirs, have showed a fuzzy-logic approach to examine the feasibility of the application of PPG signals as a new method in the identification of humans.

The PPG signals were acquired from the fingertips of 17 healthy subjects and were used as fuzzy entries for the classification of four distinctive features. The rate of success in the fuzzy-based decision can reach up to 94% in the same testing and 84% for two different trials. This outcome suggests that this new PPG-based biometry is potentially feasible in the verification of humans [17].

In another study, the design of an amplifier circuit intended for extracting the DC component of the signal is being negotiated for PPG signals. Consequently, a high AC signal with SNR (signal-to-noise ratio) is acquired from a raw PPG signal, adding a bias-adjusted circuit to the amplifier. This hardware development resulted in acquiring a better signal quality and a data handling convenience in recognition (identification) [18].

In another study, it was emphasized that the finger print of someone could be imitated by placing a thin film or using the artificial copy of that print in a biometric system operating via finger scanning. This study researches into the possibility to utilize the PPG signal as an additional parameter along with the finger print. The uniqueness of a finger impact profile was approved in the preliminary studies [19].

Venkatasubramanian et al., in their studies, stated that body area networks (BAN) could play an important role in tracking the health conditions of soldiers in the battle field. A secure BAN is required to maintain the security of soldiers. This research offers a key agreement protocol referred to as PPG-based PKA. This study shows the feasibility of PPG signals to communicate over a common symmetrical encoding key between two spots within BAN [20].

Humphreys et al., in their studies, developed and tested an image-based PPG system against the fingertip-based one often used in the conventional clinical practices. Since a direct contact with the tissue is required in conventional applications, performing such practices on a lesion makes them impossible to apply. So as to cope with this inadequacy, a CMOS camera –based system selecting the PPG signal without contacting the tissue was developed. The comparison of the conventional methods and the conclusions yielded perfect results [21].

In another study, a contact-free reflection PPG (NRPPG) is being developed for the purpose of monitoring the PPG signal features

and comparing it with a contact PPG (CPPG). The CPPG and NRPPG signals acquired simultaneously from 22 healthy subjects are studied. The power spectrums of these PPG signals are compared among themselves and analyzed. The results suggest that NRPPG can be used in the evaluation of cardio-physiological signals [22].

In yet another study, a CMOS camera-based imaging PPG system (PPGI) is identified to perceive the blood vibrations in the tissue. PPGI draws the attention to the potential applications in the visualized blood flow. The change in the density of three wavelengths (600 nm, 520 nm and 432 nm) is perceived within each pixel of the image and analyzed. Special image processing software was developed in order to obtain a two-dimensional map of the blood flow measurements of the skin. High definition PPGI images are derived from human fingers (by transmission mode) and from face (by reflection mode) through evaluating them with these three wavelengths. This newly-developed system could be useful in tracking the skin blood flow for clinical applications [23].

In another study, it is cited that the optical sensors in which photons are used as the detectors are becoming increasingly significant in a non-invasive identification area. When compared with EEG, MRI and FMRI, they are relatively cheap, easy-to-use and easy -to-install. Among many optical sensors, PPG (photoplethysmography) sensors have the ability to measure the blood volume changes of subcutaneous veins. The objective is the identifying parameters like the heart rate and the respiratory rate. The heart rate can be measured by the real-time PPG signals obtained from the sensors. The detailed analyses of the frequency spectrum of PPG signal suggest a cardiac peak at about 1 Hz for 60 heartbeats a minute and a respiratory peak at about 0.25 Hz for 15 inhalation a minute [24].

Ram et al., in their studies, have emphasized that the performances of pulse oximetres are highly influenced by the motion artifacts (MA) getting involved in the PPG signal. As a simple and efficient approach, they propose an adaptive step-size least mean squares (AS-LMS) adaptive filter for reducing MA s in corrupted PPG signals [25].

In another study, on the other hand, while getting the PPG signal, the most appropriate position for the sensor can be found out by researching a low DC deviation in the signal. The AC component is great in a position where the DC fluctuation is small in the recommended PPG. Of the four blood vessels, dorsal, palmer, ulnar and radial vessel areas, small DC amplitude and large AC amplitude were observed in the ulnar vessel area [26].

3. Materials and methods

3.1. PPG biometrics dataset

In this study, PPG signals were acquired from a total of thirty healthy volunteers, seventeen of whom are male and thirteen of whom are female as shown in Table 1. The data were obtained from their right index fingers while they were seated in a calm position.

Prior to the acquisition of data, information regarding the study was given to the volunteers, the questions they were curious about were answered, the explanations as to the privacy of the data and their personal information and keeping them within the limits of scientific studies were made, and they were given a form to fill out the information about their consent and approval of volunteering to participate in this study. A 15-period-signal (each) was acquired from each individual at two different time spans. 40 characteristic features were extracted for each period. The *Z*-score method was used in standardizing these characteristic feature variables. The 1st configuration data set with the characteristic features acquired by the first received signals from the subjects, the 2nd configuration data set with the characteristic features received at a different time later on and a 3rd configuration data set by combining these two data sets were built up. In order to enable the permanency of the characteristic features acquired from the volunteers to be evaluated with more than one example within a given time in due course, datasets of the 1st configuration and the 2nd configuration were created. A dataset of the 3rd configuration was created to be able to identify the characteristic features which had duration in time. In Fig. 2, the acquisition of PPG signal from a volunteer is demonstrated.

3.2. The proposed PPG biometrics recognition system

In this study, the system, the block diagram of which is shown in Fig. 3 is recommended. In this system were the PPG signals acquired by a PPG data acquisiton card with a STM32F103xC ARM

Table 1
Descriptive statistics for male and female groups.

Groups	Age (years)	Height (cm)	Weight (kg)	Smoking	No-smoking	BMI (kg/m^2)
Mean ± **SD** (range) for males	28.41 ± 8.68 (18–46)	175 ± 7.62 (164–190)	81 ± 16.95 (61–125)	10	7	26.4 ± 4.26 (20.1–35.7)
Mean ± **SD** (range) for females	26.46 ± 8.18 (18–42)	161 ± 4.88 (155–171)	61 ± 6.76 (52–75)	3	10	23.4 ± 2.8 (19.1–29.3)
Mean ± **SD** (range) for total	27.57 ± 8.38 (18–46)	169 ± 9.3 (155–190)	72 ± 16.69 (52–125)	13	17	25.1 ± 3.9 (19.1–35.7)

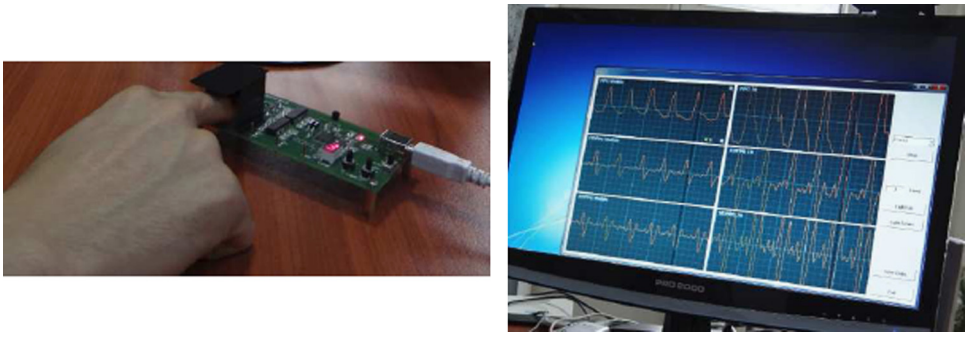

Fig. 2. The acquisition of PPG signal from the volunteers.

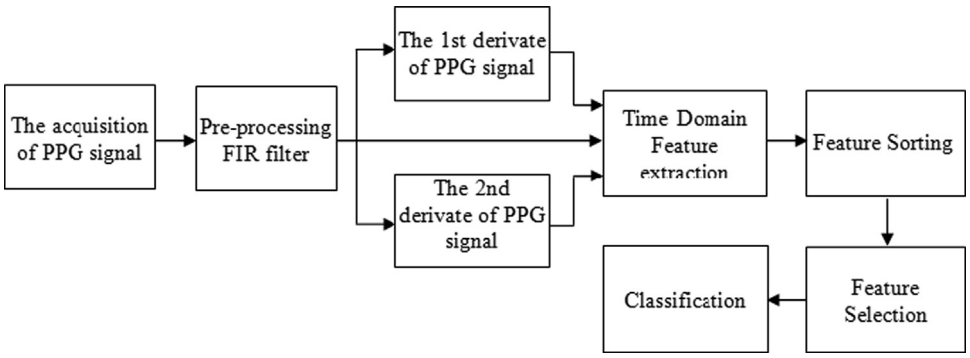

Fig. 3. The block diagram of biometric identity authentication system based on PPG signal.

based 32 bit microcontroller and a 2 kHz sampling frequency, and on which there is a DCM03 reflective sensor. In order to debug the noises in the PPG signal as a pre-processing, a FIR low-pass filter with $N=$ 200 points 10 Hz cut-off frequency was utilized. The first and the second derivatives are calculated via the filtered PPG signal.

40 time domain features are acquired by normalizing the filtered PPG and its derivatives to the range of 0–1. These characteristic features are used for the purpose of classification after the feature ranking and feature selection processes, respectively.

3.2.1. *Differentiation stage*

The formula for differentiation has to provide three characteristics for one-dimensional digital signals:

1. Both the first and the second derivatives should be zero where the function is constant.
2. The first derivative should be constant and the second derivative should be zero for the decreasing and increasing beams.
3. At the beginning of the decreasing and increasing curves, the first derivative should be different from zero, and the second derivative, on the other hand, should be different from zero both at the beginning and the end of them.

These are the three characteristics of the common math differentiation.

Considering these characteristics, the derivative for one-dimensional signals can be calculated as follows:

$$\text{1st derivative}: \quad \frac{\partial f}{\partial x} = f(x+1) - f(x) \tag{1}$$

$$\text{2nd derivative}: \quad \frac{\partial^2 f}{\partial x^2} = f(x+1) + f(x-1) - 2f(x) \tag{2}$$

In Fig. 4, the first and the second derivative applications for a one-dimensional signal are shown.

3.2.2. *Feature extraction stage: time domain features*

At this stage, characteristic features are extracted from PPG signal and its first and second derivatives. In Figs. 5 and 6, the relation between PPG signal and its first and second derivative is shown, respectively. Feature points in PPG signals are determined using these correlations.

In Figs. 7 and 8 are all the feature spots shown. The first detected feature spots are the systolic peak points. Then for the first derivative previous to the position of these systolic peak points in PPG signal, there is the first peak point which is a1; for the second derivative, there is the first peak and there are *a*2 and *b*2 points which are the first pit points. Then comes *b*1, *e*1, *f*1 points for the first derivative and *e*2 and *f*2 for the second derivative following the position of systolic peak point. By these

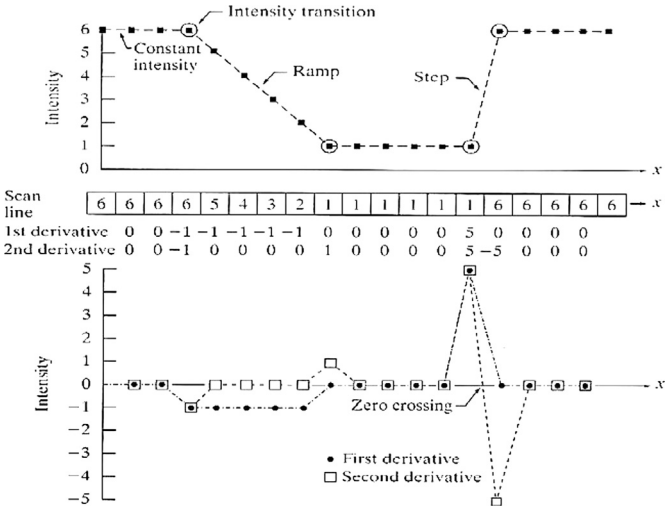

Fig. 4. First and second derivative representation for a one-dimensional digital (numeric) signal [27].

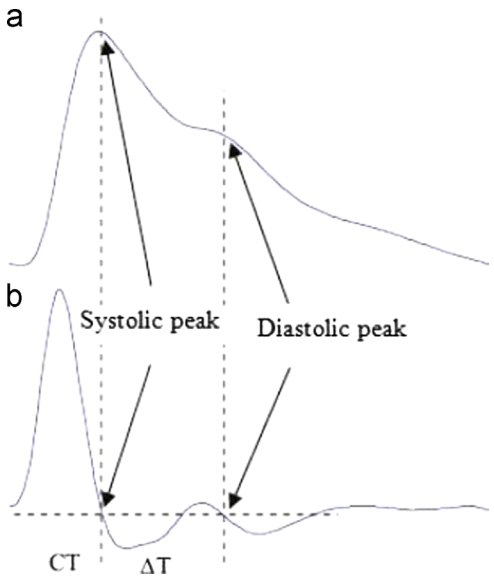

Fig. 5. Signal measurements. (a) original fingertip PPG and (b) the first derivative of PPG [28].

feature spots detected in the time domain, 40 characteristic features were calculated, such as *x* (systolic peak), *y* (diastolic peak), *z* (dicrotic notch), *tpi* (pulse interval), *tpp* (peak to peak), y/x (augmentation index), $(x-y)/x$ (alternative augmentation index), $z/x|(y-z)|/x$, *t*1 (systolic peak time), *t*2 (dicrotic notch time), *t*3

(diastolic peak time), ΔT (time between systolic and diastolic peaks), width (the pulse width with semi-height of the systolic peak), $A2/A1$ (inflection point area ratio-IPA), $t1/x$ (systolic peak output curve), $y/(tpi-t3)$ (diastolic peak downward curve), $t1/tpp$, $t2/tpp$, $t3/tpp$, $\Delta T/tpp$, $ta1$, $tb1$, $te1$, $tf1$, $b2/a2$, $e2/a2$, $(b2+c2)/a2$, $ta2$, $tb2$, $ta1/tpp$, $tb1/tpp$, $te1/tpp$, $tf1/tpp$, $ta2/tpp$, $tb2/tpp$, $(ta1-ta2)/tpp$, $(tb1-tb2)/tpp$, $(te1-t2)/tpp$, $(tf1-t3)/tpp$.

3.2.3. *Feature ranked stage: distance based supervised feature ranked algorithm*

A feature ranking algorithm is proposed for the 40 features calculated during this study. The proposed ranking algorithm is used as a matrix input which consists of n period, which has, for each period, an $\mathbf{m}-1$ different feature and classification label and which has $\mathbf{n}$ line $\mathbf{m}$ column. Our objective is to determine the features that will classify each period accurately using the distance functions and to rank the features according to the percentage of accurate classification. To that end, this feature ranking algorithm is proposed.

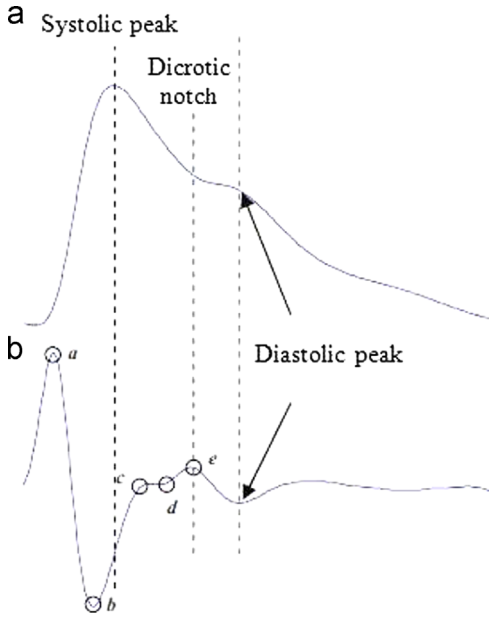

Fig. 6. Signal measurements. (a) Original fingertip PPG and (b) the second derivative of PPG [28].

Algorithm.

A1. Let the

$$X=\begin{bmatrix} x_{1,1} & \cdots & x_{1,m-1} & x_{1,m} \\ \vdots & \ddots & \vdots & \vdots \\ x_{n,1} & \cdots & x_{n,m-1} & x_{n,m} \end{bmatrix}$$

matrix be composed of the first one $(m-1)$ feature column and an m. classification label column.

A2. With the Euclidean distance formula,

$$d_{i,j}=\sqrt{\sum_{z=1}^{n}(x_{i,j}-x_{z,j})^2}, \quad \begin{matrix} i=1,2,\ldots,n \\ j=1,2,\ldots,m-1 \\ z\neq i \text{ için } z=1,2,\ldots,n \end{matrix}$$

a matrix of distances is formed in this way:

In order for the success of the classification of any feature to be high, it is expected that the distance of column elements of the same label (tag) between themselves be close to each other. For this reason, this matrix was formed.

A3. A sequence of $(n-1)$ elements is formed for $z=1, 2, \ldots, n$ provided $z\neq i$ by calculating the distance of any element of matrix D to the other column elements of the matrix with the absolute distance formula,

$$D_{d_{i,j}}(z)=|d_{i,j}-d_{z,j}|$$

A4. The item k is selected by the ascending sort of the elements of this sequence (by sorting the elements of this sequence from small to large). From this selected element k, $s_{i,j}$ score is acquired by ascertaining the class label of $d_{i,j}$. element of matrix

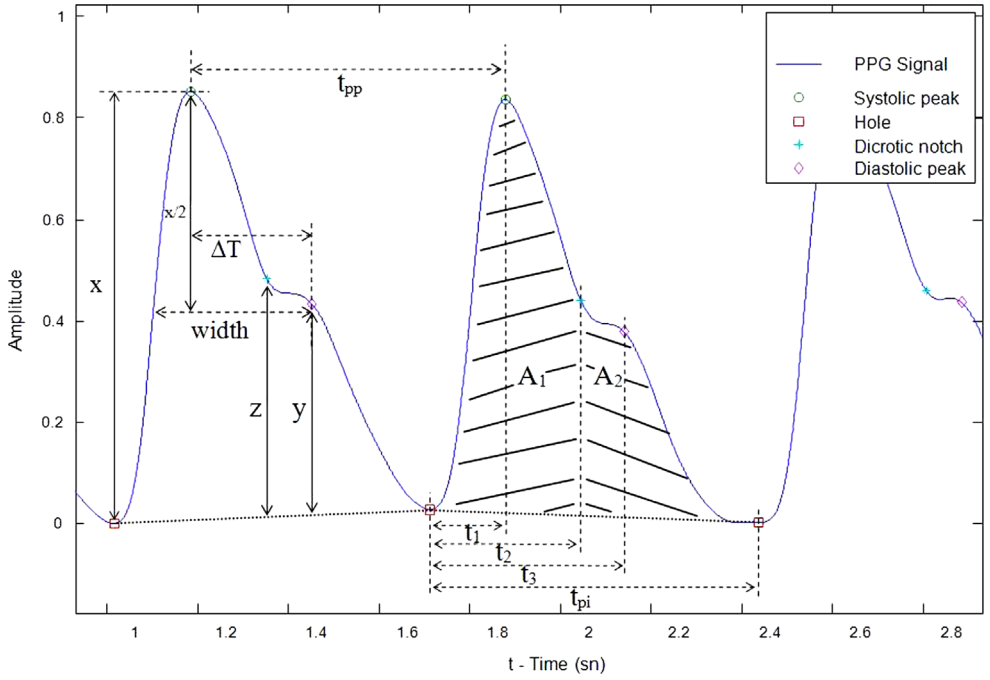

Fig. 7. PPG signal; the characteristic features acquired from PPG signal.

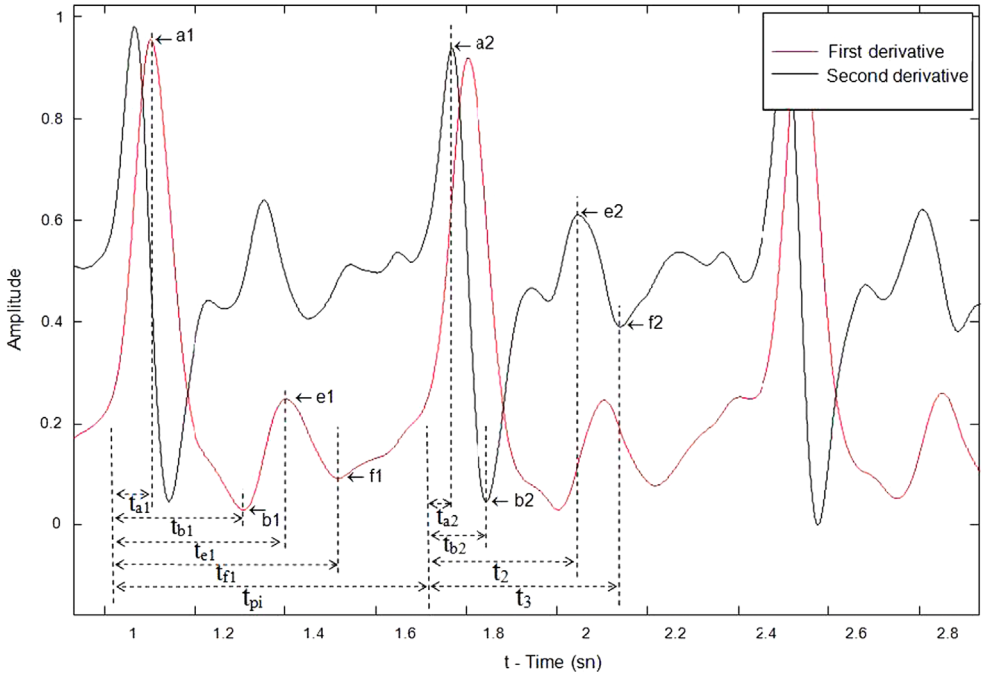

Fig. 8. The first and the second derivatives of PPG signal; the characteristic features acquired from the derivatives.

Table 2
The ranked features for the 1st configuration.

Feature ranking algorithm *k* values for majority voting							
***k*=3**		***k*=5**		***k*=7**		***k*=10**	
% accuracy	**Ranked feature**	**% accuracy**	**Ranked feature**	**% accuracy**	**Ranked feature**	**% accuracy**	**Ranked feature**
8.59	14	6.53	14	5.97	10	6.33	10
7.11	10	5.91	10	5.81	14	5.22	14
5.85	5	5.73	37	5.49	30	4.87	5
5.78	13	5.69	13	5.24	13	4.60	13
5.41	37	5.11	30	5.17	37	4.56	37
4.96	30	4.84	5	4.60	5	4.13	30
4.59	16	4.00	4	4.19	21	3.78	21
4.44	8	3.87	21	4.10	8	3.62	4
4.44	9	3.82	8	4.10	9	3.29	24
4.15	23	3.82	9	3.52	31	3.27	8
4.07	22	3.82	16	3.49	4	3.27	9
3.85	4	3.69	22	3.49	12	3.00	31
3.63	24	3.64	23	3.43	24	2.96	32
3.63	27	3.56	31	3.40	33	2.91	33
3.56	19	3.51	24	3.17	38	2.80	27
3.48	26	3.33	33	3.05	22	2.69	29
3.48	29	3.29	12	3.02	23	2.67	12
3.48	35	3.29	35	2.76	27	2.53	16
3.19	18	3.24	29	2.76	32	2.47	22
3.11	12	3.20	27	2.57	29	2.47	38
2.96	32	3.02	32	2.54	1	2.33	23
2.89	21	2.84	26	2.54	16	2.20	39
2.89	31	2.62	1	2.48	35	2.00	35
2.89	33	2.62	19	2.44	26	1.98	36
2.81	25	2.62	38	2.06	15	1.96	1
2.67	1	2.58	39	2.03	34	1.96	19
2.59	28	2.53	18	2.00	2	1.89	17
2.52	6	2.27	6	2.00	36	1.80	18
2.52	7	2.27	7	1.90	6	1.78	26
2.52	17	2.27	15	1.90	7	1.78	40
2.52	38	2.09	2	1.90	18	1.73	15
2.52	39	2.04	40	1.90	25	1.73	34
2.37	15	1.96	17	1.87	39	1.56	2
2.37	34	1.91	28	1.75	28	1.51	6
2.37	36	1.87	34	1.71	19	1.51	7
2.37	40	1.87	36	1.49	40	1.44	20
1.93	2	1.60	25	1.40	17	1.42	25
1.93	20	1.51	20	1.24	3	1.36	28
1.48	11	1.47	11	1.11	11	1.00	3
0.96	3	1.07	3	0.92	20	0.78	11

Table 3
The selected feature numbers for the 1st configuration and the percentages of classification success depending on the changes in classification algorithm *k* values.

	The selected feature numbers							
	5	**10**	**15**	**20**	**25**	**30**	**35**	**40**
Classification algorithm *k* values	74.22	80.22	88.89	87.33	***90.44***	89.78	89.11	89.33
	74.44	78.44	86.00	85.11	89.11	87.11	88.00	87.78
	75.11	77.78	83.56	87.11	87.33	86.89	85.11	84.89
	74.22	78.89	83.11	84.00	84.89	84.22	83.33	83.78
	72.67	75.56	78.67	82.00	84.00	82.44	81.78	82.44

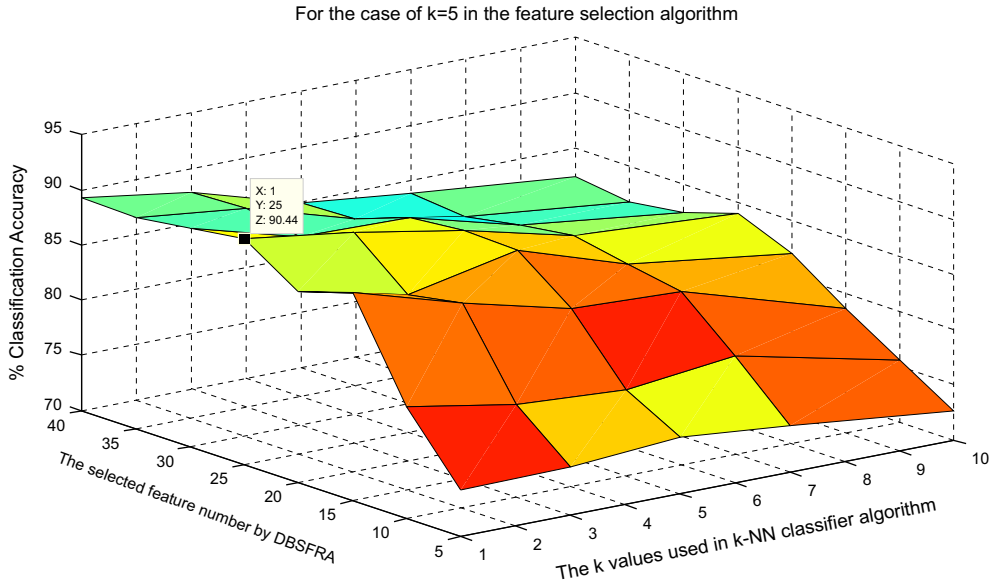

Fig. 9. The selected feature numbers for the 1st configuration and the percentages of classification success depending on the changes in classification algorithm *k* values.

Table 4
The 1st configuration performance measurement values.

Volunteer	**Precision (%)**	**Recall (%)**	**Specificity (%)**	***f*-Measure**	**Volunteer**	**Precision (%)**	**Recall (%)**	**Specificity (%)**	***f*-Measure**
1	100.00	93.33	100.00	0.97	**16**	60.00	80.00	98.16	0.69
2	93.33	93.33	99.77	0.93	**17**	100.00	100.00	100.00	1.00
3	90.91	66.67	99.77	0.77	**18**	87.50	93.33	99.54	0.90
4	93.75	100.00	99.77	0.97	**19**	100.00	100.00	100.00	1.00
5	82.35	93.33	99.31	0.88	**20**	100.00	100.00	100.00	1.00
6	91.67	73.33	99.77	0.81	**21**	100.00	86.67	100.00	0.93
7	100.00	86.67	100.00	0.93	**22**	88.24	100.00	99.54	0.94
8	87.50	93.33	99.54	0.90	**23**	87.50	93.33	99.54	0.90
9	91.67	73.33	99.77	0.81	**24**	84.62	73.33	99.54	0.79
10	100.00	86.67	100.00	0.93	**25**	70.59	80.00	98.85	0.75
11	100.00	93.33	100.00	0.97	**26**	93.75	100.00	99.77	0.97
12	92.86	86.67	99.77	0.90	**27**	100.00	100.00	100.00	1.00
13	82.35	93.33	99.31	0.88	**28**	100.00	100.00	100.00	1.00
14	77.78	93.33	99.08	0.85	**29**	100.00	86.67	100.00	0.93
15	93.33	93.33	99.77	0.93	**30**	88.24	100.00	99.54	0.94
					Average	91.26	90.44	99.67	0.90

D and the number of those which are the same. When the scores are calculated for all the elements of matrix *D*, the following matrix *S* is achieved.

In matrix *S* obtained, a sequence of $m-1$ elements is achieved by the gathering of each column elements among themselves

$$s_j = \sum_{i=1}^{n} s_{i,j} \quad j = 1, 2, \ldots, m-1 \tag{3}$$

The s_j in this sequence shows the score of *j*. feature.

While the scores of number of $m-1$ feature from $j=1$ are being lined up from great to small, the labels of features, that is to say, *m*. column lines up in the same row and an array of features ranked (AOFR) is achieved.

3.2.4. *Feature selection stage*

Counting all the features in the computation at the stage of classification may adversely affect the success of classification due

Table 5
The ranked features for the 2nd configuration.

Feature ranking algorithm *k* values for majority voting							
***k*=3**		***k*=5**		***k*=7**		***k*=10**	
% accuracy	**Ranked feature**	**% accuracy**	**Ranked feature**	**% accuracy**	**Ranked feature**	**% accuracy**	**Ranked feature**
9.33	14	7.02	14	5.81	14	5.38	14
7.48	23	5.96	22	5.56	23	5.38	23
6.89	22	5.73	26	5.11	37	5.18	30
6.30	27	5.73	30	5.02	30	4.96	37
6.00	26	5.56	37	4.79	22	4.47	24
5.93	37	5.24	23	4.73	26	4.22	10
5.70	30	4.40	24	4.60	10	3.87	26
5.33	24	4.40	29	3.84	29	3.40	4
5.04	29	4.27	10	3.75	5	3.40	16
4.37	16	4.27	27	3.71	4	3.31	5
4.37	38	4.13	4	3.62	16	3.24	8
4.30	5	4.04	38	3.59	24	3.24	9
4.22	21	3.87	16	3.52	27	3.16	12
4.15	10	3.60	33	3.49	33	3.04	33
4.00	4	3.56	5	3.30	8	3.00	3
3.93	8	3.51	8	3.30	9	3.00	22
3.93	9	3.51	9	3.05	34	2.87	29
3.70	31	3.24	28	2.92	21	2.87	40
3.56	25	3.11	31	2.92	38	2.67	11
3.48	34	2.84	25	2.83	3	2.58	21
3.41	17	2.80	12	2.76	12	2.58	28
3.26	28	2.67	3	2.70	11	2.49	17
2.81	11	2.67	34	2.67	40	2.40	27
2.81	18	2.62	21	2.63	28	2.33	34
2.74	12	2.49	17	2.57	25	2.27	25
2.52	33	2.44	40	2.51	31	2.22	13
2.44	15	2.40	11	2.38	13	2.16	31
2.37	3	2.18	13	2.35	17	2.00	38
2.37	32	2.04	6	2.13	19	1.98	39
2.22	39	2.04	7	1.97	39	1.58	32
2.07	40	1.91	39	1.78	15	1.53	6
1.93	6	1.87	15	1.65	32	1.53	7
1.93	7	1.82	1	1.56	18	1.49	18
1.93	19	1.73	20	1.56	36	1.47	19
1.85	20	1.69	35	1.49	6	1.47	35
1.78	13	1.69	36	1.49	7	1.24	15
1.63	36	1.64	32	1.33	20	1.16	1
1.56	1	1.56	18	1.33	35	1.04	2
1.33	35	1.51	19	1.30	1	1.04	36
1.26	2	1.29	2	1.02	2	0.80	20

to redundant and irrelevant features. At the stage of feature ranking, such redundant and irrelevant features rank last in AOFR.

In this stage of study, the first 5, 10, 15, 20, 25, 30, 35 and 40 features from the ranked ones are selected and several classification accomplishments are made for $k=1$, 3, 5, 7, 10 values by means of k-nearest neighbor classification method. The number of features yielding the best classification achievement and k value are selected as the classifier model.

In this case, a decision as to how many of the ranked features must be selected first should be made. In particular, the reason for the first ranked ones to be 5, 10, …, 40 during the selection is to allow for a less amount of time for the processing time. Here, if required, the selection can be made in the form of 1, 2, 3, …, 40, however, the processing time will multiply fivefold. Of these ranked features selected, the step value in the form of the first 5 features can be put to the user request. This process has been suggested as a method of research for the best classification performance.

3.2.5. Classification stage: distance based classifier algorithms

This is the process of determining what individuals the input signals of the utilized methods belong to in cases where the characteristic feature points obtained from the classification input signals are qualitative. The purpose, here, is to identify the class label of the input signal in a space of a given number classes. The concept of similarity is usually defined by the reversal of distance. In the distance-based classification, minimum distance is used for high similarity. The most popular method performing classification by utilizing the distances between the characteristic feature points is the *k*-nearest neighbors algorithm.

***k*-Nearest neighbors algorithm**

- *k* value is arbitrarily determined.
- The distances between the characteristic feature points with unknown class labels and those with the known class labels are calculated. In general, the Euclidean distance is utilized.
- The calculated distances are ranked. The closest *k* number of class labels with the smallest distance are ascertained.
- Among the *k* number of class labels ascertained, the one with the majority is determined. This determined class label is assigned as the outcome of the unknown class.

In order for the classification success to be assessed objectively, methods referred to as cross validation should be applied. In these methods, the data contained within the system are divided in two

as the training dataset and the testing dataset. The training data are used to train the system, whereas the testing data are utilized to evaluate the success of the trained system. In the literature, three types of cross validation methods are proposed:

- Repeated random sub-sampling validation;
- *K*-fold cross-validation;
- Leave-one-out cross-validation.

In the repeated random sub-sampling validation, the training and testing data are randomly selected from the dataset. This is the method ensuring the highest level of success within the cross validation.

In the *K*-fold cross-validation, the dataset is divided into *k* pieces of folds. One fold is used for the testing data, and the remaining $K-1$ folds are combined and employed as training data. This process is repeated *K* times through the transposition of the

Table 6
The selected feature numbers for the 2nd configuration and the percentages of classification success depending on the changes in classification algorithm *k* values.

	The selected feature numbers							
	5	**10**	**15**	**20**	**25**	**30**	**35**	**40**
Classification algorithm *k* values	75.11	91.33	92.44	***94.44***	93.56	91.33	90.67	90.22
	73.78	91.11	91.78	92.22	91.78	90.00	90.44	90.00
	75.33	90.44	91.11	91.33	90.22	87.78	89.11	89.11
	73.56	89.56	89.33	91.11	90.00	88.00	88.89	88.22
	70.89	87.11	88.00	89.33	89.11	86.67	87.78	87.56

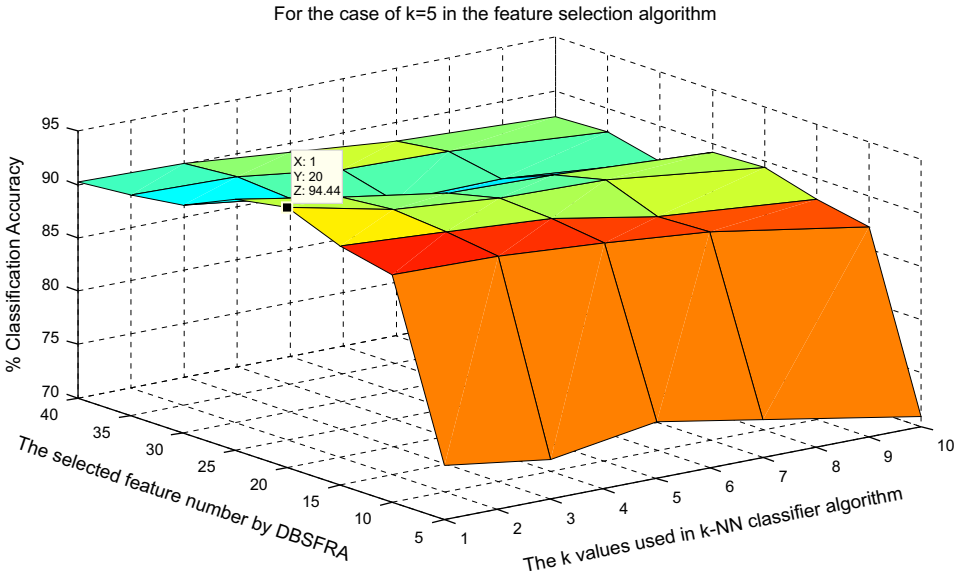

Fig. 10. The selected feature numbers for the 2nd configuration and the percentages of classification success depending on the changes in classification algorithm *k* values.

Table 7
2nd configuration performance measurement values.

Volunteer	**Precision (%)**	**Recall (%)**	**Specificity (%)**	***f*-Measure**	**Volunteer**	**Precision (%)**	**Recall (%)**	**Specificity (%)**	***f*-Measure**
1	100.00	100.00	100.00	1.00	**16**	100.00	100.00	100.00	1.00
2	92.86	86.67	99.77	0.90	**17**	100.00	93.33	100.00	0.97
3	100.00	100.00	100.00	1.00	**18**	100.00	93.33	100.00	0.97
4	93.33	93.33	99.77	0.93	**19**	100.00	100.00	100.00	1.00
5	78.95	100.00	99.08	0.88	**20**	93.75	100.00	99.77	0.97
6	100.00	93.33	100.00	0.97	**21**	100.00	100.00	100.00	1.00
7	100.00	66.67	100.00	0.80	**22**	100.00	100.00	100.00	1.00
8	88.24	100.00	99.54	0.94	**23**	100.00	100.00	100.00	1.00
9	87.50	93.33	99.54	0.90	**24**	87.50	93.33	99.54	0.90
10	100.00	93.33	100.00	0.97	**25**	93.75	100.00	99.77	0.97
11	100.00	93.33	100.00	0.97	**26**	100.00	100.00	100.00	1.00
12	92.31	80.00	99.77	0.86	**27**	88.24	100.00	99.54	0.94
13	92.86	86.67	99.77	0.90	**28**	93.75	100.00	99.77	0.97
14	77.78	93.33	99.08	0.85	**29**	87.50	93.33	99.54	0.90
15	100.00	100.00	100.00	1.00	**30**	100.00	80.00	100.00	0.89
					Average	94.94	94.44	99.81	0.94

Table 8
The ranked features for the 3rd configuration.

Feature ranking algorithm *k* values for majority voting							
***k*=3**		***k*=5**		***k*=7**		***k*=10**	
% accuracy	**Ranked feature**	**% accuracy**	**Ranked feature**	**% accuracy**	**Ranked feature**	**% accuracy**	**Ranked feature**
5.26	14	4.56	37	4.38	37	3.89	10
5.15	23	4.51	14	3.83	10	3.68	37
4.67	37	3.93	23	3.65	30	3.18	30
4.44	24	3.67	10	3.52	23	3.11	23
4.30	29	3.33	30	3.25	14	2.88	26
4.22	10	3.13	26	3.13	26	2.64	14
4.15	22	3.02	29	2.70	27	2.60	5
3.85	26	3.00	5	2.65	22	2.38	22
3.63	16	3.00	22	2.56	5	2.36	27
3.56	17	2.91	16	2.54	8	2.34	8
3.52	5	2.91	24	2.54	9	2.34	9
3.11	8	2.73	13	2.37	13	2.22	24
3.11	9	2.67	8	2.37	16	2.14	29
3.07	25	2.67	9	2.37	24	2.12	13
3.04	13	2.58	27	2.30	25	2.06	4
3.00	30	2.31	17	2.27	29	2.02	25
2.67	38	2.24	25	2.00	4	1.81	16
2.56	19	2.20	35	1.97	38	1.80	38
2.52	35	2.18	38	1.92	17	1.78	21
2.48	34	2.07	4	1.90	21	1.77	31
2.37	39	2.04	19	1.90	35	1.69	17
2.30	11	1.89	12	1.86	31	1.69	34
2.30	15	1.87	31	1.86	33	1.63	12
2.22	21	1.80	11	1.71	32	1.63	19
2.19	4	1.76	21	1.70	12	1.53	1
2.19	18	1.76	32	1.67	19	1.50	32
2.19	28	1.67	6	1.52	11	1.49	33
2.19	31	1.67	7	1.52	34	1.40	35
2.04	1	1.67	34	1.49	1	1.34	11
2.00	27	1.64	1	1.35	6	1.28	6
1.93	12	1.64	18	1.35	7	1.28	7
1.93	33	1.62	28	1.30	18	1.23	40
1.78	36	1.49	33	1.25	40	1.21	18
1.70	6	1.38	36	1.24	36	1.13	28
1.70	7	1.38	39	1.16	20	1.11	15
1.63	40	1.36	40	1.16	28	1.11	36
1.52	32	1.29	3	1.11	3	1.09	39
1.48	3	1.20	15	1.06	15	1.07	3
1.37	20	1.16	20	0.98	39	1.01	20
1.11	2	0.87	2	0.79	2	0.81	2

Table 9
The selected feature numbers for the 3rd configuration and the percentages of classification success depending on the changes in classification algorithm *k* values.

	The selected feature numbers							
	5	**10**	**15**	**20**	**25**	**30**	**35**	**40**
Classification algorithm *k* values	67.56	81.33	86.56	86.67	86.00	86.56	86.44	84.22
	65.67	79.44	***87.22***	85.44	84.33	85.44	85.67	83.22
	65.89	80.11	86.33	83.33	83.22	83.56	83.78	80.89
	64.33	78.44	85.00	82.78	82.89	81.89	83.44	80.44
	62.56	76.89	82.00	81.67	80.44	80.00	82.00	79.67

sets. For the success status, the average of K number of success values is taken.

Leave-one-out cross-validation method is quite similar to the K-fold cross-validation. The leave-one-out cross-validation method for the dataset consisting of N number of samples is the application of the K-fold method as in: $K=N$.

During this stage, the k-nearest neighbor classification algorithm was used. Through leave-one-out method, the classification success was achieved. The k-nearest neighbor algorithm categorizes by means of using the distances between data points. In order to identify the class of any PPG period, separate distances are calculated between the feature spots extracted from that period and those extracted from all the PPG periods, the classes of which are known. As for distance, the Euclidean distance was used in this study. The selected number of k labels with the majority of the class label of the most closely known period was determined as the class of an unknown period.

4. Results and discussion

In this study, a classification model was built up for biometric identification, with the PPG signals acquired from 30 volunteers. 40 features were extracted using PPG signals and its derivatives.

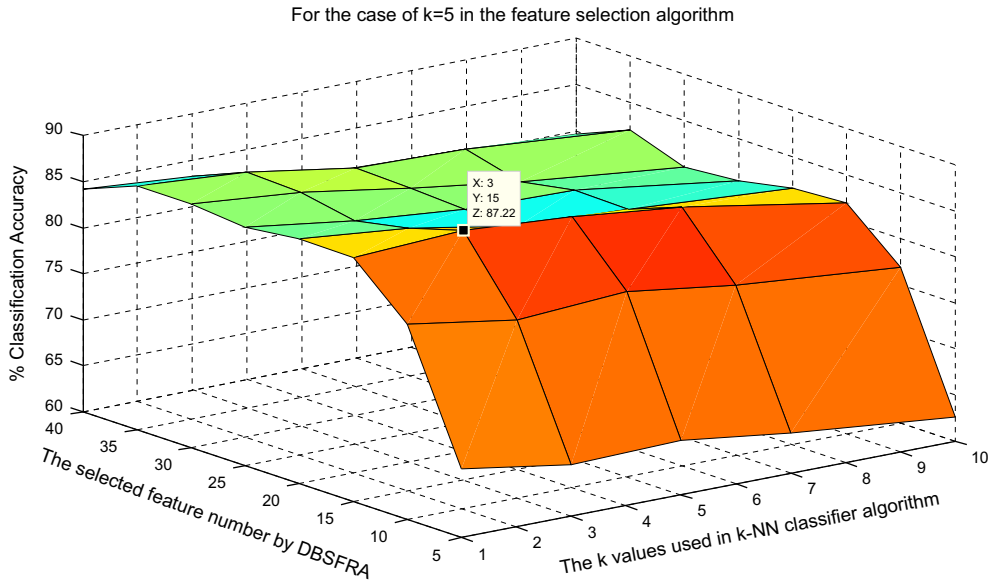

Fig. 11. The selected feature numbers for the 3rd configuration and the percentages of classification success depending on the changes in classification algorithm k values.

A feature ranking algorithm was proposed in order to rank these features. In the proposed feature ranking algorithm, $k=$ 3, 5, 7 and 10 values were applied for majority voting. The selection process, in particular, was done by picking out the first ranked 5, 10, 15, 20, 25, 30, 35 and 40 features separately and by deciding as to how many features had to be selected considering the one with the highest achievement of classification. The classification process was done by utilizing the k-nearest neighbor classifier algorithm and leave-one-out transposition for $k=1$, 3, 5, 7, and 10 values.

In Table 2, the ranked features are shown according to k values used in the feature ranking algorithm for the 1st configuration. The percentages of classification success are shown in Table 3. The percentages of classification success are calculated using the ranked features for $k=5$ value in Table 2. The best classification success was achieved as 90.44% for $k=1$ value of the classification algorithm where the first 25 features were used. Besides, it is seen that when there is no feature selection and ranking process in Table 3, a 89.33% of classification success at most could be achieved for the classification algorithm $k=1$ value in the event that all the features are used. In this case, a 1.11% of increase in the classification success was attained through the feature ranking and selection process for the 1st configuration. The percentages of classification success for the 1st configuration are graphically shown in Fig. 9. The performance measurement values calculated from this matrix, such as precision, recall, specificity and f-measure, are shown in Table 4.

Similarly, in Table 5, the ranked features according to the k values used in the feature ranking algorithm are shown for the 2nd configuration. In Table 6 are the percentages of classification success shown. They are calculated using the ranked features for $k=5$ value in Table 5. The best classification success was achieved as 94.44% for $k=1$ value of the classification algorithm where the first 20 features were used. Besides, it is seen that when there is no feature selection and ranking process in Table 6, a 90.22% of classification success at most could be achieved for the classification algorithm $k=1$ value in the event that all the features are used. In this case, a 4.22% of increase in the classification success was attained through the feature ranking and selection process for the 2nd configuration. The percentages of classification success for the 2nd configuration are graphically shown in Fig. 10. The performance measurement values calculated from this matrix, such as precision, recall, specificity and f-measure are shown in Table 7.

Similarly, in Table 8, the ranked features according to the k values used in the feature ranking algorithm are shown for the 3rd configuration. In Table 9 are the percentages of classification success shown. They are calculated using the ranked features for $k=5$ value in Table 8. The best classification success was achieved as 87.22% for $k=3$ value of the classification algorithm where the first 15 features were used. Besides, it is seen that when there is no feature selection and ranking process in Table 9, a 84.22% of classification success at most could be achieved for the classification algorithm $k=1$ value in the event that all the features are used. In this case, a 3% of increase in the classification success was attained through the feature ranking and selection process for the 3rd configuration. The percentages of classification success for the 3rd configuration are graphically shown in Fig. 11. The performance measurement values calculated from this matrix, such as precision, recall, specificity and f-measure are shown in Table 10.

When Tables 2 and 6 are compared, the ranking of 40 features acquired for the 1st configuration and the 2nd configuration is not the same, which suggests that the features could rank differently in achieving the best performance depending on time. Since the 3rd configuration is formed by the combination of the 1st configuration and the 2nd configuration, the features ranked in Table 10 are more accurate than those in Tables 2 and 6 in the evaluation of the features with duration in time.

The diagrams in Figs. 12 and 13 are given in order to demonstrate, for biometric recognition, the availability of the major features extracted as time-domain from the PPG signal. In Fig. 12, according to the first three major features selected through DBSFRA for the 1st configuration, the 2nd configuration and the 3rd configuration, the distributions of classification of 6 individuals are shown. In Fig. 13, on the other hand, The PPG signal periods of an individual and the alteration of the major features selected through DBSFRA among these periods are separately depicted for the 1st configuration, the 2nd configuration and the 3rd configuration.

The physical descriptions of some features between the obtained ranked 15 features for the best performance in the 3rd configuration are given in Table 11.

5. Conclusions and future works

In this study, 40 characteristic features were acquired using the PPG signal and its first and second derivatives. A system intended for the application of these features was performed for biometric identity authentication. The duration of the 40 features received from the volunteers within this proposed system was evaluated through two samples different from each other in time.

Table 10
3rd configuration performance measurement values.

Volunteer	Precision (%)	Recall (%)	Specificity (%)	f-measure	Volunteer	Precision (%)	Recall (%)	Specificity (%)	f-measure
1	80.56	96.67	99.20	0.88	**16**	72.22	86.67	98.85	0.79
2	92.86	86.67	99.77	0.90	**17**	96.67	96.67	99.89	0.97
3	81.82	60.00	99.54	0.69	**18**	87.10	90.00	99.54	0.89
4	90.32	93.33	99.66	0.92	**19**	100.00	100.00	100.00	1.00
5	85.29	96.67	99.43	0.91	**20**	87.88	96.67	99.54	0.92
6	100.00	73.33	100.00	0.85	**21**	90.00	90.00	99.66	0.90
7	88.00	73.33	99.66	0.80	**22**	88.24	100.00	99.54	0.94
8	88.89	80.00	99.66	0.84	**23**	93.55	96.67	99.77	0.95
9	76.67	76.67	99.20	0.77	**24**	70.83	56.67	99.20	0.63
10	80.00	80.00	99.31	0.80	**25**	84.38	90.00	99.43	0.87
11	90.63	96.67	99.66	0.94	**26**	93.10	90.00	99.77	0.92
12	85.19	76.67	99.54	0.81	**27**	96.77	100.00	99.89	0.98
13	80.65	83.33	99.31	0.82	**28**	93.33	93.33	99.77	0.93
14	75.00	90.00	98.97	0.82	**29**	87.10	90.00	99.54	0.89
15	93.55	96.67	99.77	0.95	**30**	92.31	80.00	99.77	0.86
					Average	87.43	87.22	99.56	0.87

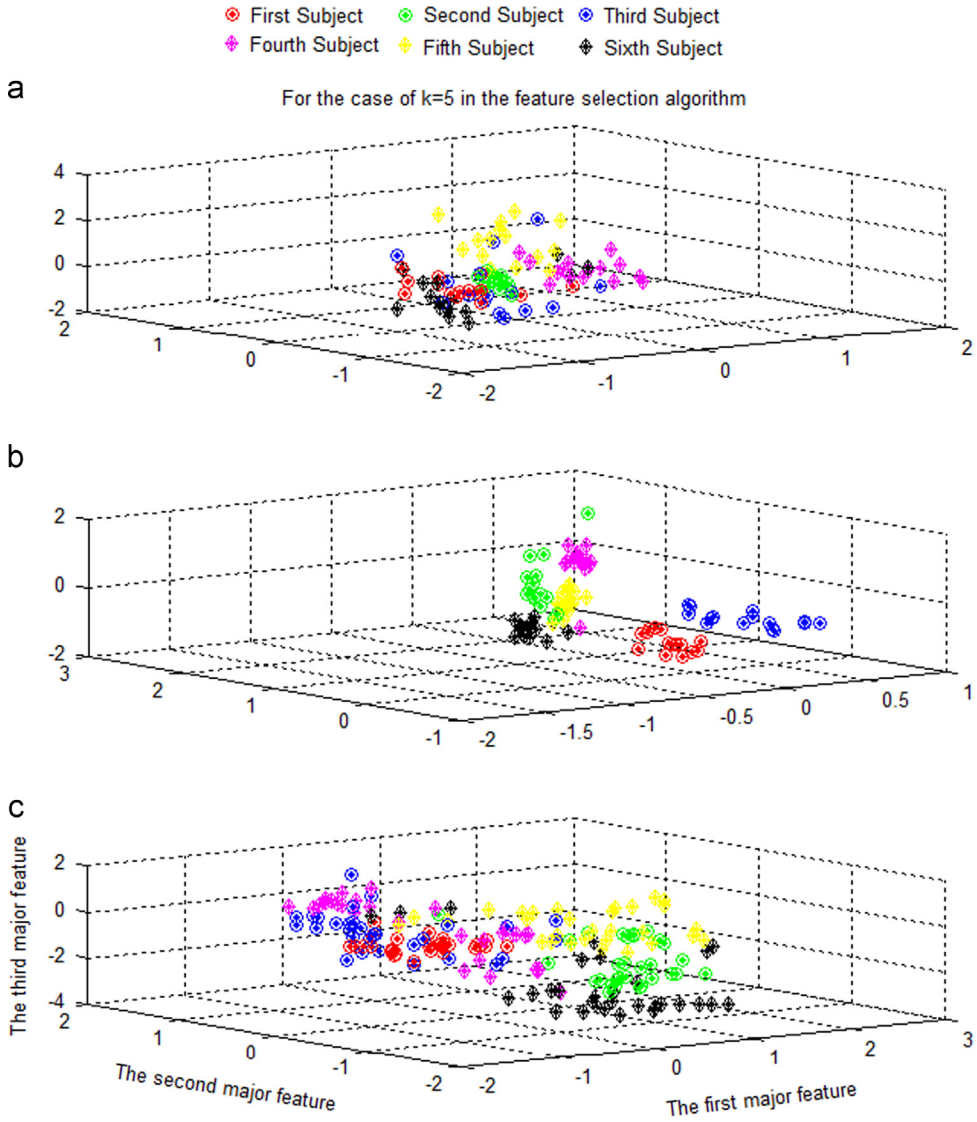

Fig. 12. The class distributions of six people according to the first three major features selected through DBSFRA. (a) The class distribution for the 1st configuration. (b) The class distribution for the 2nd configuration. (c) The class distribution for the 3rd configuration.

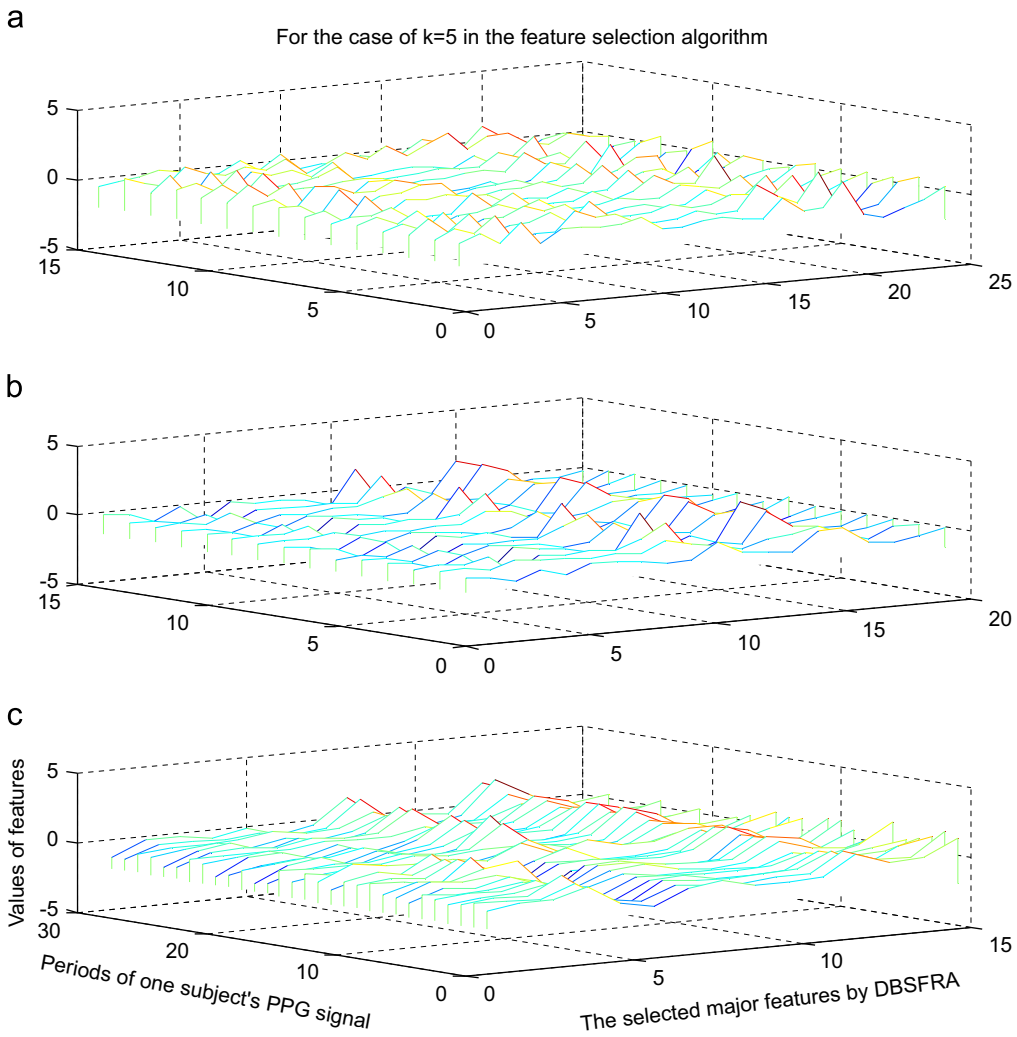

Fig. 13. The PPG signal periods of an individual and the alteration of the major features selected through DBSFRA among these periods. (a) The alteration of the major features for the 1st configuration. (b) The alteration of the major features for the 2nd configuration. (c) The alteration of the major features for the 3rd configuration.

Table 11
The physical descriptions of some features between the obtained ranked 15 features for the best performance in the 3rd configuration.

Feature numbers	Features	Physical description
14	*t*1 (systolic peak time)	Alty et al. [29] proved that the crest time is a useful feature for cardiovascular disease classification. They developed a method to classify subjects into high and low pulse wave velocity (equivalent to high and low cardio vascular disease risk) using features extracted from the PPG
26	*b*2/*a*2	Takazawa et al. [30] demonstrated that the b/a ratio reflects increased arterial stiffness, hence the *b*/*a* ratio increases with age. Imanaga et al. [31] provided a direct evidence that magnitude of b/a of the APG is related to the distensibility of the peripheral artery, and suggest that the magnitude of b/a is a useful non-invasive index of atherosclerosis and altered arterial distensibility Aiba et al. [32] suggested the parameter -b/a in the exposure group dose dependently decreased with increases in length of working career (duration of exposure to lead) and blood lead concentration (Pb–B). The parameter $-b/a$ significantly decreased in subjects with working careers of 5 years or more and in subjects whose Pb–B was 40 g/100 ml or more. While Nousou et al. [33] found that the b/a index discriminates independently between subjects with essential hypertension and healthy controls Otsuka et al. [34] found that the *b*/*a*, is positively correlated to the Framingham risk score. Framingham risk score has been used to estimate individual risk of cardiovascular heart disease. Their results suggest that b/a index might contribute to the discrimination of the high-risk subjects for cardiovascular heart disease Baek et al. [35] confirmed that the *b*/*a* ratio increases with age
5	Peak to peak *tpp*	The R–R interval in the ECG signal correlates closely with the peak–peak interval APG signal as both represent a completed heart cycle. The peak–peak interval has been used to detect the heart in PPG signals [36,37]
13	IPA=*A*2/*A*1	Wang et al. [38] have divided the pulse area into two areas at the dicrotic notch. They found that the ratio of the two areas, can be used as an indicator of total peripheral resistance. This ratio is called the inflection point area ratio (IPA)
27	*e*2/*a*2	Takazawa et al. [30] demonstrated that an increase of the e/a ratio reflects decreased arterial stiffness, and that the e/a ratio decreases with age. Baek et al. [35] confirmed that the e/a ratios decreases with age

At this stage, our experimental studies have been confined to these mentioned so far as this has been the first study of ours we have been working on. The feature points to be acquired in consequence of the evaluations to be performed through further examples different from each other in time would be a more accurate approach in achieving the best result for identity authentication. It was observed that the feature ranking and selection algorithm we proposed boosted the classification success of the system. Moreover, the rates of success provided here are found by means of separately assessing each period acquired from the volunteers. In fact, it is seen that while performing identity authentication, success will be boosted further when authentication is performed by taking into consideration the majority voting of more than one period to be received from an individual. The results obtained suggest that the use of the PPG signal for biometric authentication is very promising. In our prospective studies, we will be increasing the success for the matter involved by also carrying out frequency-based analyses as well as the features acquired from PPG signals at time domain.

Conflict of interest statement

None declared.

Acknowledgment

This work was supported by Research Fund of the Sakarya University. Project Number: 2014-50-02-006 entitled “Biometric Identification System with PPG (Photeplethysmography) Signals”.

References

[1] Y.Y. Gu, Y. Zhang, Y.T. Zhang, A novel biometric approach in human verification by photoplethysmographic signals, in: 4th International IEEE EMBS Special Topic Conference on Information Technology Applications in Biomedicine, 24–26 April 2003, pp. 13–14.
[2] R. Brunelli, T. Poggio, Face recognition: features versus templates, Pattern Anal. Mach. Intell. IEEE Trans. 15 (October (10)) (1993) 1042–1052.
[3] A. Samal, P.A. Iyengar, Automatic recognition and analysis of human faces and facial expressions: a survey, Pattern Recognition 25 (1992) 65–67.
[4] D. Dumn, Using a multi-layer perceptron neural for human voice identification, in: Proceedings of the 4th International Conference on Signal Processing, Applications and Technology, Newton, MA, USA, 1993.
[5] M. Negin, T.A. Chmielewski, M. Salganicoff, U.M von Seelen, P.L. Venetainer, G. G. Zhang, An iris biometric system for public and personal use, Computer 33 (2) (2000) 70–75.
[6] Kyong Seok Paik, Chin Hyan Chung, Jin Ok Kim, Dae Jun Hwang, On a lip print recognition by the pattern kernels with multiresolution architecture, in: Proceedings of International Conference on Image Processing, vol. 2, 2001, pp. 246–249.
[7] ChewYean Yam, M.S. Nixon, J.N. Carter, Performance analysis on new biometric gait motion model, in: Proceedings of the 5th IEEE Southwest Symposium on Image Analysis and Interpretation, 2002, pp. 31–34.
[8] R.B. Paranjape, J. Mahovsky, L. Benedicenti, Z. Koles', The electroencephalogram as a biometric, in: Canadian Conference on Electrical and Computer Engineering, vol. 2, 2001, pp. 1363–1366.
[9] L. Biel, O. Pettersson, L. Philipson, P. Wide, ECG analysis: a new approach in human identification, IEEE Trans. Instrum. Meas. 50 (3) (2001) 808–812.
[10] L. Biel, O. Pettersson, L. Philipson, P. Wide, ECG analysis: a new approach in human identification, in: IMTC/99, Proceedings of the 16th IEEE Instrumentation and Measurement Technology Conference, vol. 1, 1999, pp. 557–561.
[11] T.W. Shen, W.J. Tompkins, Y.H. Hu, One-lead ECG for identity verification, in: 2nd Joint Conference of the IEEE Engineering in Medicine and Biology Society and the Biomedical Engineering Society, Huston, 2002.
[12] J. Bailey, M. Fecteau, N.L. Pendleton, Wireless Pulse Oximeter (Bachelor Degree Thesis), Worcester Polytechnic Institute, April 24, 2008.
[13] Advanced Prime Materials Korea ⟨http://www.apmkr.com/⟩ (accessed July, 2013).
[14] Jianchu Yao, Xiaodong Sun, Yongbo Wan, A pilot study on using derivatives of photoplethysmographic signals as a biometric identifier, in: 29th Annual International Conference of the IEEE Engineering in Medicine and Biology Society, 2007 (EMBS 2007), 22–26 August 2007, pp. 4576–4579.
[15] P. Spachos, Jiexin Gao, D. Hatzinakos, Feasibility study of photoplethysmographic signals for biometric identification, in: 2011 17th International Conference on Digital Signal Processing (DSP), 6–8 July 2011, pp. 1–5.
[16] Chen Wei, Lei Sheng, Guo Lihua, Chen Yuquan, Pan Min, Study on conditioning and feature extraction algorithm of photoplethysmography signal for physiological parameters detection, in: 2011 4th International Congress on Image and Signal Processing (CISP), vol. 4, 15–17 October 2011, pp. 2194–2197.
[17] Y.Y. Gu, Y.T. Zhang, Photoplethysmographic authentication through fuzzy logic, in: IEEE EMBS Asian-Pacific Conference on Biomedical Engineering, 20–22 October 2003, pp. 136–137.
[18] Yongbo Wan, Xiaodong Sun, Jianchu Yao, Design of a photoplethysmographic sensor for biometric identification, in: International Conference on Control, Automation and Systems, 2007 (ICCAS'07), 17–20 October 2007, pp. 1897–1900.
[19] M. Singh, S. Gupta, “Correlation studies of PPG finger pulse profiles for Biometric system”, Int. J. Inf. Technol. Knowl. Manage. 5 (January–June (1)) (2012) 1–3.
[20] K.K. Venkatasubramanian, A. Banerjee, S. Gupta, Plethysmogram-based secure inter-sensor communication in body area networks, in: IEEE Military Communications Conference, 2008 (MILCOM 2008), 16–19 November 2008, pp. 1–7.
[21] K. Humphreys, C. Markham, T. Ward, A CMOS camera-based system for clinical photoplethysmographic applications, Proc. SPIE 5823 (2005) 88–95.
[22] P. Shi, S. Hu, Y. Zhu, J. Zheng, V. Azorin-Peris, A. Echiadis, Development of a remote photoplenthysmographic technique for human biometrics, in: Proceedings of the SPIE BiOS, Photonics West, San Jose, USA, vol. 7169-41, 2009.
[23] U. Rubins, R. Erts, V. Nikiforovs, The blood perfusion mapping in the human skin by photoplethysmography imaging, in: MEDICON 2010, IFMBE Proceedings, vol. 29, 2010, pp. 304–306.
[24] L. Rutuja, D. Nivedita, Applications of finger photoplethysmography, Int. J. Eng. Res. Appl. 2 (1) (2012) 877–880.
[25] M.R. Ram, K.V. Madhav, E.H. Krishna, N.R. Komalla, K.A. Reddy, A novel approach for motion artifact reduction in PPG signals based on AS-LMS adaptive filter, IEEE Trans. Instrum. Meas. 61 (5) (2012) 1445–1457.
[26] L. Chungkeun, S.S. Hang, P. Jongchul, L. Myoungho, The optimal attachment position for a fingertip photoplethysmographic sensor with low DC, IEEE Sens. J. 12 (May (5)) (2012) 1253–1254.
[27] R.C. Gonzalez, R.E. Woods, Digital İmage Processing, Prentice-Hall, 2008.
[28] M. Elgendi, On the analysis of fingertip photoplethysmogram signals, Curr. Cardiol. Rev. 8 (1) (2012) 14–25.
[29] SR Alty, N Angarita-Jaimes, SC Millasseau, PJ. Chowienczyk, Predicting arterial stiffness from the digital volume pulse waveform, IEEE Trans. Biomed. Eng. 54 (12) (2007) 2268–2275.
[30] K TN Takazawa, M Fujita, O Matsuoka, T Saiki, M Aikawa, S Tamura, C. Ibukiyama, Assessment of vasocative agents and vascular aging by the second derivative of photoplethysmogram waveform, Hypertension 32 (1998) 365–370.
[31] I Imanaga, H Hara, S Koyanagi, K. Tanaka, Correlation between wave components of the second derivative of plethysmogram and arterial distensibility, Jpn. Heart J. 39 (1998) 775–784.
[32] Y Aiba, S Ohshiba, S Horiguchi, I Morioka, K Miyashit, I Kiyota, et al., Peripheral hemodynamics evaluated by acceleration plethysmography in workers exposed to lead, Ind. Health 37 (1999) 3–8.
[33] N. Nousou, S. Urase, Y. Maniwa, K. Fujimura, Y. Fukui, Classification of acceleration plethysmogram using self-organizing map, in: International Symposium on Intelligent Signal Processing and Communications, 2006 (ISPACS '06), 2006, pp. 681–684.
[34] T Otsuka, T Kawada, M Katsumata, C. Ibuki, Utility of second derivative of the finger photoplethysmogram for the estimation of the risk of coronary heart disease in the general population, Circ. J. 70 (2006) 304–310.
[35] H.J. Baek, J.S. Kim, Y.S. Kim, H.B. Lee, K.S. Park, Second derivative of photoplethysmography for estimating vascular aging, in: The 6th International Special Topic Conference on Information Technology Applications in Biomedicine, 2007, pp. 70–72.
[36] W.M. Jubadi, S.F.A. Mohd Sahak, Heartbeat monitoring alert via SMS, in: IEEE Symposium on Industrial Electronics & Applications, 2009.
[37] E Gil1, M Orini1, R Bail´on, J Vergara, L Mainardi, P. Laguna, Photoplethysmography pulse rate variability as a surrogate measurement of heart rate variability during non-stationary conditions, Physiol. Meas. 31 (9) (2010) 127–1290.
[38] L. Wang, E. Pickwell-MacPherson, Y.P. Liang, Y.T. Zhang, Noninvasive cardiac output estimation using a novel photoplethysmogram index, in: Annual International Conference of the IEEE Engineering in Medicine and Biology Society, 2009.